Electronic Research Archive

http://www.aimspress.com/journal/era

ERA, 32(1): 293–316.
DOI: 10.3934/era.2024014
Received: 29 August 2023
Revised:19 November 2023
Accepted: 21 November 2023
Published: 25 December 2023

Research article

Bifurcation analysis of a two–dimensional p53 gene regulatory network without and with time delay

Xin Du[1], Quansheng Liu[1,*] and Yuanhong Bi[2,3]

[1] School of Mathematical Sciences, Inner Mongolia University, Hohhot 010021, China
[2] School of Statistics and Mathematics, Inner Mongolia University of Finance and Economics, Hohhot 010070, China
[3] Inner Mongolia Key Laboratory for Economic Data Analysis and Mining, Hohhot 010070, China

* **Correspondence:** Email: smslqs@imu.edu.cn; Tel: +8618947166686.

Abstract: In this paper, the stability and bifurcation of a two–dimensional p53 gene regulatory network without and with time delay are taken into account by rigorous theoretical analyses and numerical simulations. In the absence of time delay, the existence and local stability of the positive equilibrium are considered through the Descartes' rule of signs, the determinant and trace of the Jacobian matrix, respectively. Then, the conditions for the occurrence of codimension–1 saddle–node and Hopf bifurcation are obtained with the help of Sotomayor's theorem and the Hopf bifurcation theorem, respectively, and the stability of the limit cycle induced by hopf bifurcation is analyzed through the calculation of the first Lyapunov number. Furthermore, codimension-2 Bogdanov–Takens bifurcation is investigated by calculating a universal unfolding near the cusp. In the presence of time delay, we prove that time delay can destabilize a stable equilibrium. All theoretical analyses are supported by numerical simulations. These results will expand our understanding of the complex dynamics of p53 and provide several potential biological applications.

Keywords: stability; saddle–node bifurcation; Hopf bifurcation; Bogdanov–Takens bifurcation; time delay

1. Introduction

Dynamical analysis of gene regulatory networks (GRNs) characterized by mathematical models plays an important role in understanding the underlying mechanism of the corresponding biological processes and predicting what will happen [1–3]. A GRN is composed of genes, RNAs, and proteins represented by nodes, which are connected through the edges that indicate the transformation, promotion, and inhibition between them [4]. The expression level of proteins in the GRN is closely related to the mechanisms of a number of biochemical processes, including cell differentiation [5–7], neural plasticity [8–10] and the development of cancer [11–13]. Typically, cell fates in response to stresses are closely related to the dynamics of the tumor suppressor protein p53 in p53 GRN with core p53–Mdm2 feedback loops [14, 15]. p53 maintains a low level under a homeostatic condition while moderate and high stresses make p53 exhibit oscillation and high level, which lead to cell cycle arrest and apoptosis [16,17], respectively. Therefore, more and more research has been focusing on exploring p53 dynamics numerically and theoretically through the construction of mathematical models with the help of bifurcation diagrams [18, 19].

Bifurcation diagrams of mathematical models is a useful tool for analyzing the dynamics of GRN [20]. Bifurcation diagrams of p53 GRN in [16, 17, 21] display various types of bifurcation, such as codimension–1 saddle–node, Hopf bifurcation and codimension–2 Bogdanov–Takens bifurcation. Saddle–node bifurcation can generate the bistability with a low and high expression levels of p53, which results in cell survival and cell apoptosis, respectively. Hopf bifurcation can induce the appearance of a stable limit cycle [22] corresponding to the oscillation expression of p53, which result in cell cycle arrest [23]. Codimension–2 Bogdanov–Takens bifurcation may give rise to the coexistence of a stable steady state and a stable limit cycle [24], which correspond to cell survival and cell cycle arrest, respectively. Therefore, the analysis of the conditions under which these bifurcations occur can allow for a deeper understanding of cell fate decision in response to different parameters. More research has focused on bifurcation analyses of high–dimensional p53 GRNs through numerical simulations [25–27]. However, theoretical analysis of low-dimensional p53 GRNs contribute to the understanding of cell fate decisions under different conditions [28, 29].

Theoretical analyses of the bifurcation of dynamical systems described by ordinary differential equations play an important role in unveiling their complex dynamic properties. Previously, extensive effort has been devoted to bifurcation analyses of predator–prey models and SIR models of infectious diseases with various factors [30], while several recent studies have theoretically revealed the bifurcation of GRNs. These studies focus on investigating the existence and stability of possible equilibria of the system and deriving the rigorous mathematical proofs for the existence of bifurcations, such as saddle-node bifurcation, Hopf bifurcation of codimension–1 and Bogdanov–Takes bifurcation of codimension–2 or codimension–3 [31–34]. Besides, Hopf bifurcation may be caused by time delay in GRNs, and it is analyzed by studying the associated characteristic equation of the corresponding linearized system [18,35]. Although there has been much research on bifurcation analyses for p53 GRNs through numerical simulations, there is scant theoretical analyses of bifurcations of low dimensional p53 GRNs.

In this paper, we investigated the bifurcation of a two–dimensional p53 GRN without and with time delay, as described in [14], by performing rigorous mathematical analysis. Firstly, the existence of all possible positive equilibria are investigated by applying Descartes' rule of signs and the local stability of the positive equilibria are analyzed. Then, in the absence of time delay, the conditions for the appearance of codimension–1 saddle–node, Hopf bifurcation and codimension–2 Bogdanov–Takens bifurcation are derived by using Sotomayor's theorem [36], Hopf bifurcation theorem [37] and the normal form method, respectively, and the first Lyapunov number is calculated to obtain the stability of the limit cycle. Furthermore, in the presence of time delay, the Hopf bifurcation induced by time delay is analyzed on the basis of the Hopf bifurcation theorem. These theoretical results are numerically supported by bifurcation diagrams and phase portraits, and they can be considered as a complement to existing literature on the dynamics of p53 GRN.

The organization of this paper is as follows. The mathematical model of the p53 GRN is given in Section 2. The existence and local stability of positive equilibria of the p53 GRN without time delay are analyzed in Section 3. Section 4 presents the conditions for the occurrence of codimension–1 saddle–node bifurcation, Hopf bifurcation and codimension–2 Bogdanov–Takens bifurcation of the p53 GRN without time delay through theoretical analyses, which are supported by bifurcation diagrams and phase portraits. Section 5 is devoted to the analysis of Hopf bifurcation induced by time delay. We end the paper with the conclusion in Section 6.

2. The model of the p53 GRN

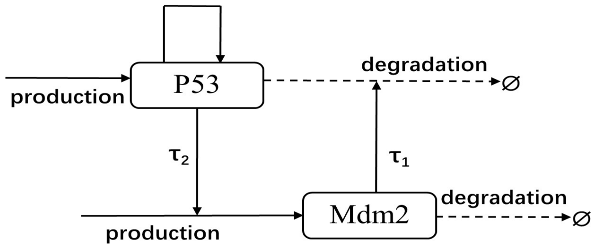

Figure 1. Schematic representation of the p53 GRN. Solid lines represent the promotion and production. Dashed lines denote the degradation with the degradation product ∅.

In the present work, we consider a core p53 GRN with p53 and its key regulator Mdm2 in [14, 15], as shown in Figure 1. Figure 1 includes a p53 self–induction positive feedback loop and a negative feedback loop, where p53 elevates the expression level of the Mdm2 protein and Mdm2 promotes the degradation of p53. Here, the degradation of p53 is regulated by the concentration of Mdm2 at some previous time. The rate equations for the concentration of p53 (denoted by x) and that of Mdm2 (denoted by y) are given by the following delay different equations:

$$\begin{cases} \dfrac{\mathrm{d}x}{\mathrm{d}t} = r_1 + v_1 \dfrac{x^2}{k_1^2 + x^2} - v_2 y(t-\tau_1) \dfrac{x}{k_2 + x} - d_1 x, \\ \dfrac{\mathrm{d}y}{\mathrm{d}t} = r_2 + v_3 \dfrac{x(t-\tau_2)^2}{k_3^2 + x(t-\tau_2)^2} - d_2 y. \end{cases} \tag{2.1}$$

Here, r_1 and r_2 denote the basal production rates of p53 and Mdm2, respectively. Also the production of both p53 and Mdm2 activated by p53 are modeled by using Hill functions with the production rates v_1 and v_3, and Michaelis constants k_1 and k_3, respectively. d_1 and d_2 are the basal degradation rates of p53 and Mdm2, respectively. Besides, p53 is degraded by Mdm2 at a rate v_2 in a Michaelis–Menten function with the Michaelis constant k_2. Time delays τ_1 and τ_2 characterize the periods of time for gene expression to protein production of p53 and Mdm2.

3. Analysis of the positive equilibria

In this section, the existence and stability of the positive equilibria of the system (2.1) are investigated and the qualitative behavior of the system (2.1) are given in the following subsections.

3.1. Existence of the positive equilibria

In the section, we focus on analyzing the conditions for the existence of a positive equilibrium in the system (2.1) for biological reasons. Assuming a positive equilibrium of the system (2.1) is $E(x_*, y_*)$, which satisfies the following equations:

$$\begin{cases} f_1(x_*, y_*) = r_1 + v_1 \dfrac{x_*^2}{k_1^2 + x_*^2} - v_2 y_* \dfrac{x_*}{k_2 + x_*} - d_1 x_* = 0, \\ f_2(x_*, y_*) = r_2 + v_3 \dfrac{x_*^2}{k_3^2 + x_*^2} - d_2 y_* = 0. \end{cases} \tag{3.1}$$

Obviously, the second equation of Eq (3.1) is equivalent to

$$y^* = \frac{r_2}{d_2} + v_3 \frac{x_*^2}{d_2(k_3^2 + x_*^2)}. \tag{3.2}$$

Rearranging the first equation of Eq (3.1), we get

$$g(x_*) = \frac{F(x_*)}{S(x_*)} = 0, \tag{3.3}$$

where

$$F(x_*) = C_6 x_*^6 + C_5 x_*^5 + C_4 x_*^4 + C_3 x_*^3 + C_2 x_*^2 + C_1 x_* + C_0, \tag{3.4}$$

$$S(x_*) = d_2(k_1^2 + x_*^2)(k_2 + x_*)(k_3^2 + x_*^2), \tag{3.5}$$

$$\begin{aligned} &C_0 = d_2 k_1^2 k_2 k_3^2 r_1,\ C_1 = k_1^2 k_3^2 (d_2 r_1 - r_2 v_2 - d_1 d_2 k_2), \\ &C_2 = d_2 k_1^2 k_2 r_1 + k_3^2 (d_2 k_2 r_1 + d_2 k_2 v_1 - d_1 d_2 k_1^2), \\ &C_3 = -k_1^2 v_2 v_3 + k_3^2 (d_2 v_1 + d_2 r_1 - r_2 v_2 - d_1 d_2 k_2) + k_1^2 (d_2 r_1 - r_2 v_2 - d_1 d_2 k_2), \\ &C_4 = -d_1 d_2 k_3^2 + (d_2 k_2 r_1 + d_2 k_2 v_1 - d_1 d_2 k_1^2), \\ &C_5 = d_2 r_1 + d_2 v_1 - r_2 v_2 - v_2 v_3 - d_1 d_2 k_2,\ C_6 = -d_1 d_2. \end{aligned} \tag{3.6}$$

Obviously, x_* is the root of the following equation

$$F(x) = 0. \tag{3.7}$$

If the root x_* of Eq (3.7) is positive, y_* is positive according to Eq (3.2) with positive rate constants. Therefore, the conditions for the existence of positive roots of Eq (3.7) are suitable for the one of the positive equilibria of the system (2.1).

Applying Descartes' rule of signs to Eq (3.7), we obtained the number of possible positive equilibria in the system (2.1) is concluded in Table 1. Obviously, the system (2.1) must have at least one positive equilibrium for $C_0C_6 < 0$. Besides, according to Eq (3.6), we conclude that if $C_2 < 0$, then $C_4 < 0$ and if $C_4 > 0$, then $C_2 > 0$. Hence, based on the cases 1–4 in Table 1, a unique positive equilibrium $E(x_*, y_*)$ in the system (2.1) exists under the conditions in the following theorem.

Table 1. Number of possible positive equilibria in the system (2.1).

Case	C_0	C_1	C_2	C_3	C_4	C_5	C_6	*Number of sign changes*	*Number of possible positive equilibria*(E)
1	+	−	−	−	−	−	−	1	1
2	+	+	−	−	−	−	−	1	1
3	+	+	+	−	−	−	−	1	1
4	+	+	+	+	−	−	−	1	1
5	+	+	+	+	+	−	−	1	1
6	+	+	+	+	+	+	−	1	1
7	+	+	−	+	−	−	−	3	1, 3
8	+	−	−	+	−	−	−	3	1, 3
9	+	−	+	+	−	−	−	3	1, 3
10	+	−	−	−	−	+	−	3	1, 3
11	+	+	−	−	−	+	−	3	1, 3
12	+	+	+	−	+	+	−	3	1, 3
13	+	−	+	+	+	+	−	3	1,3
14	+	+	+	−	+	−	−	3	1, 3
15	+	+	+	+	−	+	−	3	1, 3
16	+	−	+	+	+	−	−	3	1, 3
17	+	+	+	−	−	+	−	3	1, 3
18	+	−	+	−	−	−	−	3	1, 3
19	+	+	−	+	−	+	−	5	1, 3, 5
20	+	−	+	−	−	+	−	5	1, 3, 5
21	+	−	+	+	−	+	−	5	1, 3, 5
22	+	−	−	+	−	+	−	5	1, 3, 5
23	+	−	+	−	+	−	−	5	1, 3, 5
24	+	−	+	−	+	+	−	5	1, 3, 5

Theorem 3.1. *The system* (2.1) *has a unique positive equilibrium* $E(x_*, y_*)$ *if one of the following conditions holds:*
(i) $C_2 < 0, C_3 < 0, C_5 < 0$;
(ii) $C_1 > 0, C_3 > 0, C_4 > 0$;
(iii) $C_1 > 0, C_2 > 0, C_4 < 0, C_5 < 0$.

Theorem 3.1 is verified by the nullclines of x and y in Figure 2, where the system (2.1) has a unique positive equilibrium for the condition (i) $C_2 = -0.1197 < 0$, $C_3 = -0.1384 < 0$, $C_5 = -0.000723 < 0$ with $v_1 = 0.18$, $v_2 = 0.003$, $v_3 = 0.6$, $d_1 = 0.034$, $d_2 = 0.02$, $r_1 = 0.01$, $r_2 = 0.001$, $k_1 = 6$, $k_2 = 4$, $k_3 = 4$ in Figure 2(a) and the condition (ii) $C_1 = 0.0057 > 0$, $C_3 = 0.1080 > 0$, $C_4 = 0.0024 > 0$ with $v_1 = 0.63$, $v_2 = 0.01$, $v_3 = 0.985$, $d_1 = 0.004$, $d_2 = 0.0025$, $r_1 = 0.021$, $r_2 = 0.0001$, $k_1 = 1.5$, $k_2 = 2$, $k_3 = 9$ in Figure 2(b). Besides, Figure 2(c) shows that the system (2.1) has three positive equilibria for $C_1 = -0.1585 < 0$, $C_2 = 0.0932 > 0$, $C_3 = 0.0173 > 0$, $C_4 = -0.0107 < 0$, $C_5 = -0.0018 < 0$ in case 9 with $v_1 = 0.18$, $v_2 = 0.01$, $v_3 = 0.55$, $d_1 = 0.034$, $d_2 = 0.03$, $r_1 = 0.011$, $r_2 = 0.001$, $k_1 = 2.4$, $k_2 = 2$, $k_3 = 4$.

Here, the conditions for the existence of the positive equilibria in system (2.1) are given in Table 1. Furthermore, the stability of the positive equilibria is analyzed in the next section.

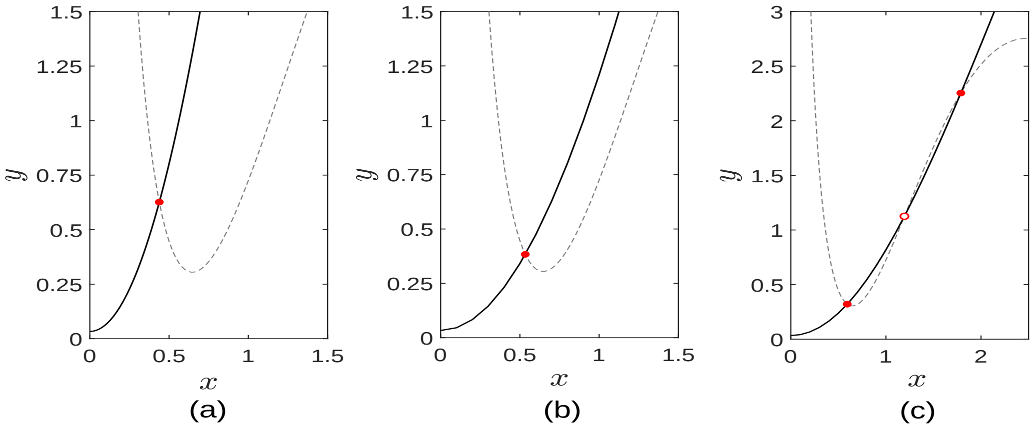

Figure 2. The nullclines of x (solid line) and y (dashed line) in system (2.1). Red solid and hollow dots are the stable and unstable equilibria.

3.2. Stability of the positive equilibria

To investigate the stability of any positive equilibrium $E(x_*, y_*)$ of the system (2.1), the corresponding Jacobian matrix J is given by

$$J(E) = \begin{pmatrix} \frac{2k_1^2 v_1 x_*}{(k_1^2 + x_*^2)^2} - \frac{k_2 v_2 y_*}{(k_2 + x_*)^2} - d_1 & -\frac{v_2 x_*}{k_2 + x_*} \\ \frac{2k_3^2 v_3 x_*}{(k_3^2 + x_*^2)^2} & -d_2 \end{pmatrix}.$$

The characteristic equation of the system (2.1) is

$$\lambda^2 - \mathrm{tr}(J)\lambda + \det(J) = 0.$$

The trace $\mathrm{tr}(J)$ and the determinant $\det(J)$ of the Jacobian matrix J are given by

$$\begin{aligned} \mathrm{tr}(J) &= \frac{2k_1^2 v_1 x_*}{(k_1^2 + x_*^2)^2} - \frac{k_2 v_2 y_*}{(k_2 + x_*)^2} - d_1 - d_2, \\ \det(J) &= \frac{k_2 v_2 d_2 y_*}{(k_2 + x_*)^2} - \frac{2k_1^2 v_1 d_2 x_*}{(k_1^2 + x_*^2)^2} + \frac{2k_3^2 v_2 v_3 x_*^2}{(k_2 + x_*)(k_3^2 + x_*^2)^2} + d_1 d_2. \end{aligned} \tag{3.8}$$

The local stability of the positive equilibrium $E(x_*, y_*)$ is decided by the signs of $\mathrm{tr}(J)$ and $\det(J)$. Next, we will first study the sign of $\det(J)$. Since

$$\begin{aligned} \det(J) =& \frac{k_2 v_2 d_2 y_*}{(k_2 + x_*)^2} - \frac{2k_1^2 v_1 d_2 x_*}{(k_1^2 + x_*^2)^2} + \frac{2k_3^2 v_2 v_3 x_*^2}{(k_2 + x_*)(k_3^2 + x_*^2)^2} + d_1 d_2 \\ =& - d_2 g'(x_*) = -d_2 \frac{F'(x_*)S(x_*) - F(x_*)S'(x_*)}{S^2(x_*)}. \end{aligned} \tag{3.9}$$

According to $F(x_*) = 0$ in Eq (3.7), we conclude that

$$\det(J) = -\frac{F'(x_*)}{(k_2 + x)(k_1^2 + x^2)(k_3^2 + x^2)}, \tag{3.10}$$

and the signs of det(J) and $F'(x_*)$ are opposite. Therefore, the signs of $F'(x_*)$ and tr(J) decide the stability of the positive equilibrium $E(x_*, y_*)$, which are given in the following theorem.

Theorem 3.2. *The stability of the positive equilibrium $E(x_*, y_*)$ under different conditions is described in Table 2.*

Table 2. The stability of the positive equilibrium $E(x_*, y_*)$.

Case	Conditions		Eigenvalues	Properties
1	$F'(x_*) < 0$	$tr(J) < 0$	$Re\lambda_1 < 0,\ Re\lambda_2 < 0$	Asymptotically stable
2		$tr(J) = 0$	$\lambda_1 = -i\sqrt{det(J)},\ \lambda_2 = i\sqrt{det(J)}$	Linear center
3		$tr(J) > 0$	$Re\lambda_1 > 0,\ Re\lambda_2 > 0$	Unstable
4	$F'(x_*) = 0$	$tr(J) < 0$	$\lambda_1 = tr(J) < 0,\ \lambda_2 = 0$	Non-hyperbolic
5		$tr(J) = 0$	$\lambda_1 = \lambda_2 = 0$	Non-hyperbolic
6		$tr(J) > 0$	$\lambda_1 = 0,\ \lambda_2 = tr(J) > 0$	Unstable(Non-hyperbolic)
7	$F'(x_*) > 0$	$\forall tr(J)$	$\lambda_1\lambda_2 < 0$	Unstable(saddle)

However, the signs of $F'(x_*)$ and tr(J) are not decided explicitly due to their complex expression, so we will give some numerical examples to illustrate the stability of $E(x_*, y_*)$ in the following section. The stability of $E(x_*, y_*)$ can be changed by the bifurcation, which will be explored in the following bifurcation analysis.

4. Bifurcation analysis of p53 GRE without time delay

Bifurcation changes the stability and the number of equilibria in the system as the parameter varies through a critical value. In this section, we investigate the conditions for the occurrence of codimension–1 saddle–node and Hopf bifurcation with respect to v_3 and codimension–2 Bogdanov–Takens bifurcation with respect to v_3 and d_2 in the system (2.1) without time delay.

4.1. Saddle-node bifurcation

According to Sotomayor theorem [36], we shall establish the conditions under which the system (2.1) experiences saddle–node bifurcation at the equilibrium $E(x_*, y_*)$ when the control parameter v_3 crosses the critical value v_3^{SN}.

The first condition is that $\mathrm{tr}(J(E))|_{v_3=v_3^{SN}} \neq 0$ and $\det(J(E))|_{v_3=v_3^{SN}} = 0$, which correspond to

$$
\textbf{(SN.1)}\quad
\begin{aligned}
&\frac{2k_1^2 v_1 x_*}{(k_1^2 + x_*^2)^2} - \frac{k_2 v_2 y_*}{(k_2 + x_*)^2} - d_1 - d_2 \neq 0,\\
&v_3^{SN} = \frac{2k_1^2 v_1 d_2 x_*(k_2 + x_*)(k_3^2 + x_*^2)^2}{2k_3^2 v_2 x_*^2 (k_1^2 + x_*^2)^2} - \frac{k_2 v_2 d_2 y_*(k_3^2 + x_*^2)^2}{2k_3^2 v_2 x_*^2 (k_2 + x_*)} - \frac{d_1 d_2 (k_2 + x_*)(k_3^2 + x_*^2)^2}{2k_3^2 v_2 x_*^2},
\end{aligned}
$$

based on Eqs (3.8) and (3.10).

Next, to obtain the transversality conditions, the eigenvectors of the matrices $J(E, v_3^{SN})$ and

$J^T(E, v_3^{SN})$ with the eigenvalue $\lambda = 0$ are given as follows, respectively,

$$V = \begin{pmatrix} V_1 \\ V_2 \end{pmatrix} = \begin{pmatrix} \dfrac{d_2(k_3^2 + x_*^2)^2}{2k_3^2 v_3^{SN} x_*} \\ 1 \end{pmatrix}, \quad W = \begin{pmatrix} W_1 \\ W_2 \end{pmatrix} = \begin{pmatrix} -\dfrac{d_2(k_2 + x_*)}{v_2 x_*} \\ 1 \end{pmatrix}.$$

Denoting $f(x, y) = (f_1(x, y), f_2(x, y))^T$,

$$f_{v_3}\left(E; v_3^{SN}\right) = \begin{pmatrix} 0 \\ \dfrac{x_*^2}{k_3^2 + x_*^2} \end{pmatrix},$$

$$D^2 f\left(E; v_3^{SN}\right)(V, V) = \begin{pmatrix} \dfrac{\partial^2 f_1}{\partial x^2} V_1^2 + 2\dfrac{\partial^2 f_1}{\partial x \partial y} V_1 V_2 + \dfrac{\partial^2 f_1}{\partial^2 y} V_2^2 \\ \dfrac{\partial^2 f_2}{\partial x^2} V_1^2 + 2\dfrac{\partial^2 f_2}{\partial x \partial y} V_1 V_2 + \dfrac{\partial^2 f_2}{\partial^2 y} V_2^2 \end{pmatrix}_{(E; v_3^{SN})}$$

$$= \begin{pmatrix} \dfrac{d_2(k_3^2 + x_*^2)^2}{2k_3^2 v_3^{SN} x_*} \left[-\dfrac{2k_2 v_2}{(k_2 + x_*)^2} + \dfrac{d_2(k_3^2 + x_*^2)^2}{2k_3^2 v_3^{SN} x_*} \left(\dfrac{k_1^2 v_1 (k_1^2 - 3x_*^2)}{(k_1^2 + x_*^2)^3} + \dfrac{k_2 v_2 y_*}{(k_2 + x_*)^3} \right) \right] \\ \dfrac{d_2^2 (k_3^2 - 3x_*^2)(k_3^2 + x_*^2)}{4k_3^2 v_3^{SN} x_*^2} \end{pmatrix}.$$

Clearly, the transversality conditions are

$$W^T f_{v_3}\left(E; v_3^{SN}\right) = \frac{x_*^2}{k_3^2 + x_*^2} \neq 0,$$

$$\textbf{(SN.2)} \qquad W^T \left[D^2 f\left(E; v_3^{SN}\right)(V, V) \right] = \frac{d_2^2 (k_3^2 + x_*^2)^2}{2k_3^2 v_3^{SN} x_*^2} \left[\frac{2k_2}{(k_2 + x_*)} + \frac{(k_3^2 - 3x_*^2)}{2(k_3^2 + x_*^2)} - \right.$$
$$\left. \frac{d_2(k_3^2 + x_*^2)^2}{2k_3^2 v_3^{SN} x_*} \left(\frac{k_1^2 v_1 (k_1^2 - 3x_*^2)(k_2 + x_*)}{v_2 (k_1^2 + x_*^2)^3} + \frac{k_2 y_*}{(k_2 + x_*)^2} \right) \right] \neq 0.$$

Therefore, based on the above analyses, we get the following theorem.

Theorem 4.1. *The system* (2.1) *experiences saddle–node bifurcation at the positive equilibrium* $E(x_*, y_*)$ *as the parameter* v_3 *crosses the critical value* v_3^{SN} *if the conditions* (**SN.1**) *and* (**SN.2**) *hold. Here* $v_3^{SN} = \frac{2k_1^2 v_1 d_2 x_* (k_2 + x_*)(k_3^2 + x_*^2)^2}{2k_3^2 v_2 x_*^2 (k_1^2 + x_*^2)^2} - \frac{k_2 v_2 d_2 y_* (k_3^2 + x_*^2)^2}{2k_3^2 v_2 x_*^2 (k_2 + x_*)} - \frac{d_1 d_2 (k_2 + x_*)(k_3^2 + x_*^2)^2}{2k_3^2 v_2 x_*^2}$.

Theorem 4.1 is verified by the bifurcation diagram of x with respect to v_3 in Figure 3(a) and phase portraits of x and y for five typical values of v_3 in Figure 3(b)–(f) with the same parameters $v_1 = 0.18$, $v_2 = 0.01$, $d_1 = 0.034$, $d_2 = 0.03$, $r_1 = 0.011$, $r_2 = 0.001$, $k_1 = 2.4$, $k_2 = 2$, $k_3 = 4$. In Figure 3(a), black solid and dashed lines represent stable and unstable equilibria, respectively, which meet at two saddle–node bifurcation points SN_1 and SN_2 with $v_3^{SN1} = 0.4606397$ and $v_3^{SN2} = 0.5991365$, respectively. In Figure 3(b)–(f), the solid lines represent the trajectory running along the arrows and red solid and hollow dots denote the stable and unstable equilibria, respectively.

As shown in Figure 3(a), the system (2.1) undergoes saddle–node bifurcation at $E_1(x_*, y_*) = (0.7593, 0.5674)$ and $E_2(x_*, y_*) = (1.3543, 2.0872)$ as v_3 passes through $v_3^{SN1} = 0.4606397$ and $v_3^{SN2} =$

0.5991365, respectively, with $\mathrm{tr}(J(E_1, v_3^{SN1})) = -0.0263 \neq 0$, $W^T\left[D^2 f\left(E_1; v_3^{SN1}\right)(V, V)\right] = 0.0118 \neq 0$ and $\mathrm{tr}(J(E_2, v_3^{SN2})) = -0.0315 \neq 0$, $W^T\left[D^2 f\left(E_2; v_3^{SN2}\right)(V, V)\right] = 0.0104 \neq 0$, which meet all conditions in Theorem 4.1. v_3^{SN1} and v_3^{SN2} divide the region in Figure 3(a) into five parts, in which phase portraits of x and y are illustrated in Figure 3(b)–(f). Only a stable equilibrium appears for $v_3 = 0.45 < v_3^{SN1}$ in Figure 3(b) and $v_3 = 0.61 > v_3^{SN2}$ in Figure 3(f). Two equilibria coexist at $v_3 = v_3^{SN1}$ in Figure 3(c) and $v_3 = v_3^{SN2}$ in Figure 3(e). There are three equilibria for v_3 that vary between v_3^{SN1} and v_3^{SN2} in Figure 3(d)).

Furthermore, the stability and property of these equilibria $E(x_*, y_*)$ in Figure 3(b)–(f) are listed in Table 3 to verify three cases in Table 2. The properties of unstable non-hyperbolic equilibria and unstable saddle are consistent with the conditions of cases 4 and 7 in Table 2, respectively. Other equilibria are asymptotically stable nodes, which correspond to case 1 in Table 2.

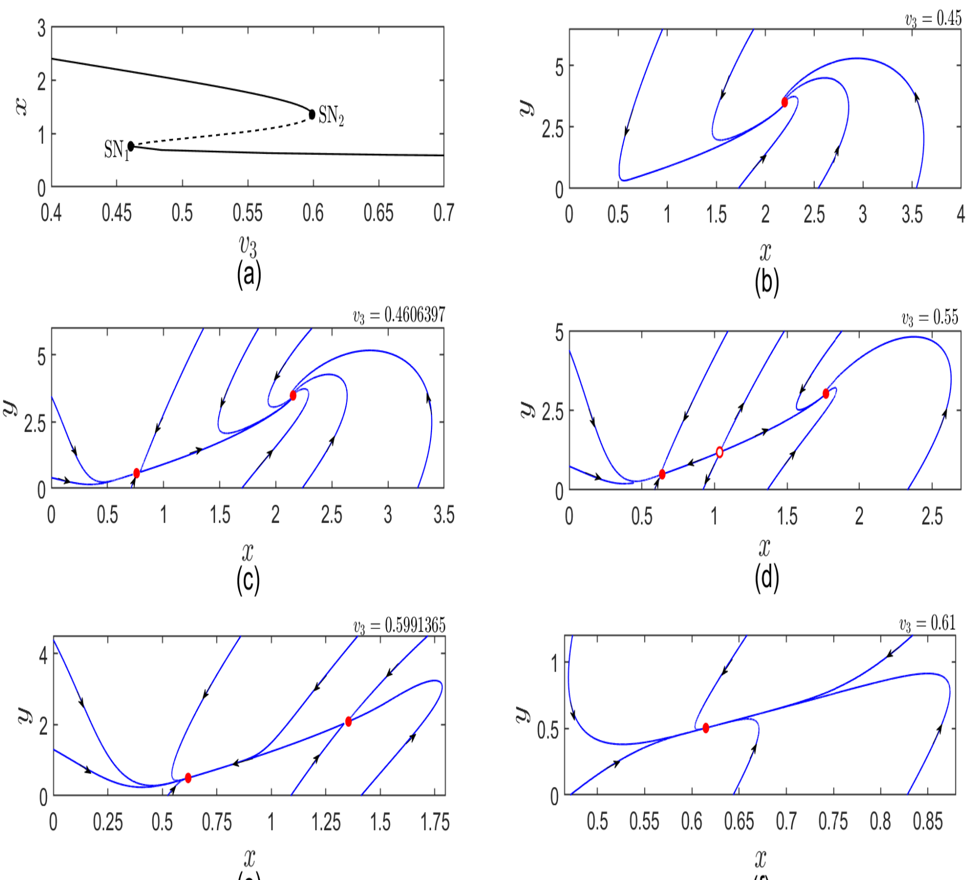

Figure 3. **(a)** Codimension–1 bifurcation diagram of x with respect to v_3 for $v_1 = 0.18$, $v_2 = 0.01$, $d_1 = 0.034$, $d_2 = 0.03$, $r_1 = 0.011$, $r_2 = 0.001$, $k_1 = 2.4$, $k_2 = 2$, $k_3 = 4$. Black solid and dashed lines represent stable and unstable equilibria, respectively. SN_1 and SN_2 are saddle–node bifurcation points. **(b)–(f)** The phase portraits of x and y for $v_3 = 0.45, 0.4606397, 0.55, 0.5991365, 0.61$, respectively. Red solid and hollow dots are stable and unstable equilibria, respectively. Blue lines with arrows denote the trajectory.

Table 3. The properties of the positive equilibria $E(x_*, y_*)$ in Figure 3.

v_3	$E_i(x_*, y_*)$	$F'(x_*)$	tr(J)	Stability	Phase portraits
0.45	(2.1967, 3.5089)	−0.2792	−0.0273	Asymptotically stable	Figure 3(*b*)
0.4606397	(0.7593, 0.5674)	0	−0.0263	Non-hyperbolic(saddle-node)	Figure 3(*c*)
	(2.1538, 3.4845)	−0.2573	−0.0267	Asymptotically stable	Figure 3(*c*)
0.55	(0.6400, 0.4910)	−0.03146	−0.0305	Asymptotically stable	Figure 3(*d*)
	(1.0352, 1.1842)	0.0246	−0.0206	Unstable(saddle)	Figure 3(*d*)
	(1.7665, 3.0254)	−0.0981	−0.0218	Asymptotically stable	Figure 3(*d*)
0.5991365	(0.6186, 0.4999)	−0.0391	−0.0315	Asymptotically stable	Figure 3(*e*)
	(1.3543, 2.0872)	0	−0.0190	Non-hyperbolic(saddle-node)	Figure 3(*e*)
0.61	(0.6147, 0.5025)	−0.0405	−0.0316	Asymptotically stable	Figure 3(*f*)

4.2. Hopf bifurcation

In this section, we try to explore the conditions under which a positive equilibrium $E(x_*, y_*)$ loses the stability through Hopf bifurcation under some parametric restriction. Here, considering v_3 as the bifurcation parameter, we shall establish the conditions under which the system (2.1) experiences Hopf bifurcation at the positive equilibrium $E(x_*, y_*)$ when v_3 crosses the critical value v_3^{HB}.

The first condition is that the Jacobian matrix $J(E, v_3^{HB})$ has a pair of purely imaginary eigenvalues, that is $\mathrm{tr}(J(E, v_3^{HB})) = 0$ and $\det(J(E, v_3^{HB})) > 0$, which correspond to

$$\textbf{(HB.1)} \qquad v_3^{HB} = -\frac{d_2(d_1 + d_2)(k_2 + x_*)^2(k_3^2 + x_*^2)}{k_2 v_2 x_*^2} + \frac{2d_2 k_1^2 v_1 x_*(k_2 + x_*)^2(k_3^2 + x_*^2)}{k_2 v_2 x_*^2(k_1^2 + x_*^2)^2} - \frac{r_2(k_3^2 + x_*^2)}{x_*^2},$$
$$\text{and } F'(x_*, v_3^{HB}) < 0.$$

Besides, the transversality condition that ensures the changes of stability of the positive equilibrium through non–degenerate Hopf bifurcation is $\dfrac{dRe(\lambda_i)}{dv_3}\,|_{v_3=v_3^{HB}} \neq 0$, i.e.,

$$\textbf{(HB.2)} \qquad \left.\frac{\mathrm{d}tr(J(E))}{\mathrm{d}v_3}\right|_{v_3=v_3^{HB}} = \frac{x_*^3(k_1^2 v_2 + v_3 x_*^2)}{F'(x_*)}\left[\frac{2k_1^4 v_1 - 6k_1^2 v_1 x_*^2}{(k_1^2 + x_*^2)^3} + \frac{k_2 r_2 v_2}{d_2(k_2 + x_*)^2} + \frac{k_2 v_2 v_3(k_3^2 + 3x_*^2 + 2x_* k_2)}{d_2(k_3^2 + x_*^2)^2(k_2 + x_*)^2}\right]$$
$$- \frac{k_2 v_2 x_*^2}{d_2(k_3^2 + x_*^2)(k_2 + x_*)^2} \neq 0.$$

Lastly, the first Lyapunov number Γ at the equilibrium $E(x_*, y_*)$ is computed to analyze the stability of the limit cycle. By the transformation $X = x - x_*$, $Y = y - y_*$, the system (2.1) becomes

$$\begin{cases} \dfrac{\mathrm{d}X}{\mathrm{d}t} = a_{10}X + a_{01}Y + a_{20}X^2 + a_{11}XY + a_{02}Y^2 + a_{30}X^3 + a_{21}X^2Y + a_{12}XY^2 + a_{03}Y^3 + Q_1(|X, Y|^4), \\ \dfrac{\mathrm{d}Y}{\mathrm{d}t} = b_{10}X + b_{01}Y + b_{20}X^2 + b_{11}XY + b_{02}Y^2 + b_{30}X^3 + b_{21}X^2Y + b_{12}XY^2 + b_{03}Y^3 + Q_2(|X, Y|^4), \end{cases}$$

where

$$a_{10} = \frac{2k_1^2 v_1 x_*}{(k_1^2 + x_*^2)^2} - \frac{k_2 v_2 y_*}{(k_2 + x_*)^2} - d_1,\ a_{01} = -\frac{v_2 x_*}{k_2 + x_*},\ a_{20} = \frac{k_1^2 v_1 (k_1^2 - 3x_*^2)}{(k_1^2 + x_*^2)^3} + \frac{k_2 v_2 y_*}{(k_2 + x_*)^3},$$
$$a_{30} = -\frac{4k_1^2 v_1 x_* (k_1^2 - x_*^2)}{(k_1^2 + x_*^2)^4} - \frac{k_2 v_2}{(k_2 + x_*)^4},\ a_{11} = -\frac{k_2 v_2}{(k_2 + x_*)^2},\ a_{21} = \frac{k_2 v_2}{(k_2 + x_*)^3},$$
$$b_{10} = \frac{2k_3^2 v_3 x_*}{(k_3^2 + x_*^2)^2},\ b_{01} = -d_2,\ b_{20} = \frac{k_3^2 v_3 (k_3^2 - 3x_*^2)}{(k_3^2 + x_*^2)^3},\ b_{30} = -\frac{4k_3^2 v_3 x_* (k_3^2 - x_*^2)}{(k_3^2 + x_*^2)^4},$$
$$a_{02} = a_{12} = a_{03} = b_{02} = b_{11} = b_{03} = b_{12} = b_{21} = b_{03} = 0.$$

According to the formula in [21], the first Lyapunov number Γ is given as follows

$$(\mathbf{HB.3}) \qquad \Gamma = -\frac{3}{2a_{01}\Phi^{\frac{3}{2}}}[a_{10}b_{10}a_{11}^2 - 2a_{10}a_{01}a_{20}^2 - 2a_{01}^2 a_{20}b_{20} - (a_{01}b_{10} - 2a_{10}^2)a_{11}a_{20} + (3a_{01}a_{30} - 2a_{10}a_{21})(a_{10}^2 + a_{01}b_{10})],$$

where $\Phi = a_{10}b_{01} - a_{01}b_{10}$.

Therefore, we get the following theorem.

Theorem 4.2. *The system* (2.1) *experiences Hopf bifurcation at the positive equilibrium $E(x_*, y_*)$ when v_3 crosses the critical value v_3^{HB} with the conditions* (**HB.1**) *and* (**HB.2**). *A supercritical (subcritical) Hopf bifurcation occurs for the first Lyapunov number* $\Gamma < 0$ (> 0) *in* (**HB.3**). *Here* $v_3^{HB} = -\frac{d_2(d_1+d_2)(k_2+x_*)^2(k_3^2+x_*^2)}{k_2 v_2 x_*^2} + \frac{2d_2 k_1^2 v_1 x_*(k_2+x_*)^2(k_3^2+x_*^2)}{k_2 v_2 x_*^2 (k_1^2+x_*^2)^2} - \frac{r_2(k_3^2+x_*^2)}{x_*^2}$.

Note that the sign of the first Lyapunov number Γ cannot be determined directly due to its complex expression; we illustrate Hopf bifurcation of the system (2.1) through the following numerical examples to verify the correctness of Theorem 4.2.

Two supercritical Hopf bifurcation points HB_{sup1} and HB_{sup2}, and a subcritical Hopf bifurcation point HB_{sub} are shown in bifurcation diagrams of x with respect to v_3 in Figure 4(a)–(b), where black solid and dashed lines respectively represent stable and unstable equilibria while green and purple lines denote stable and unstable limit cycles. For $v_1 = 0.8153$, $v_2 = 0.2$, $d_1 = 0.015$, $d_2 = 0.04$, $r_1 = 0.03$, $r_2 = 0.002$, $k_1 = 7$, $k_2 = 3$ and $k_3 = 7$, the first critical value $v_3^{HB} = 0.2096$ labeled by HB_{sup1}, where the conditions, $E(x_*, y_*) = (5.1628, 1.8957)$, $F'(x_*) = -34.7231 < 0$, $\frac{\mathrm{d}tr(J(E))}{\mathrm{d}v_3} = 0.1612 > 0$ and $\Gamma = -0.1455 < 0$, imply the appearance of a stable limit cycle. Then the stable limit cycle disappears at another critical value $v_3^{HB} = 0.2589$ labeled by HB_{sup2} with $E(x_*, y_*) = (3.3111, 1.2332)$, $F'(x_*) = -19.3163 < 0$, $\frac{\mathrm{d}tr(J(E))}{\mathrm{d}v_3} = -0.2941 < 0$ and $\Gamma = -0.9058 < 0$. For $v_3 = 0.25$ between HB_{sup1} and HB_{sup2}, a stable limit cycle surrounding an unstable equilibrium is illustrated in the phase portrait of x and y in Figure 4(c). Beside, Figure 4(b) shows a subcritical Hopf bifurcation point HB_{sub} at $v_3^{HB} = 0.1852$ with the conditions $E(x_*, y_*) = (4.4394, 4.1289)$, $F'(x_*) = -2.1014 < 0$, $\frac{\mathrm{d}tr(J(E))}{\mathrm{d}v_3} = 2.7028 > 0$ and $\Gamma = 0.4856 > 0$. An unstable limit cycle surrounding a stable focus coexists with a saddle and a node for $v_3 = 0.1838$ in the phase portrait in Figure 4(d).

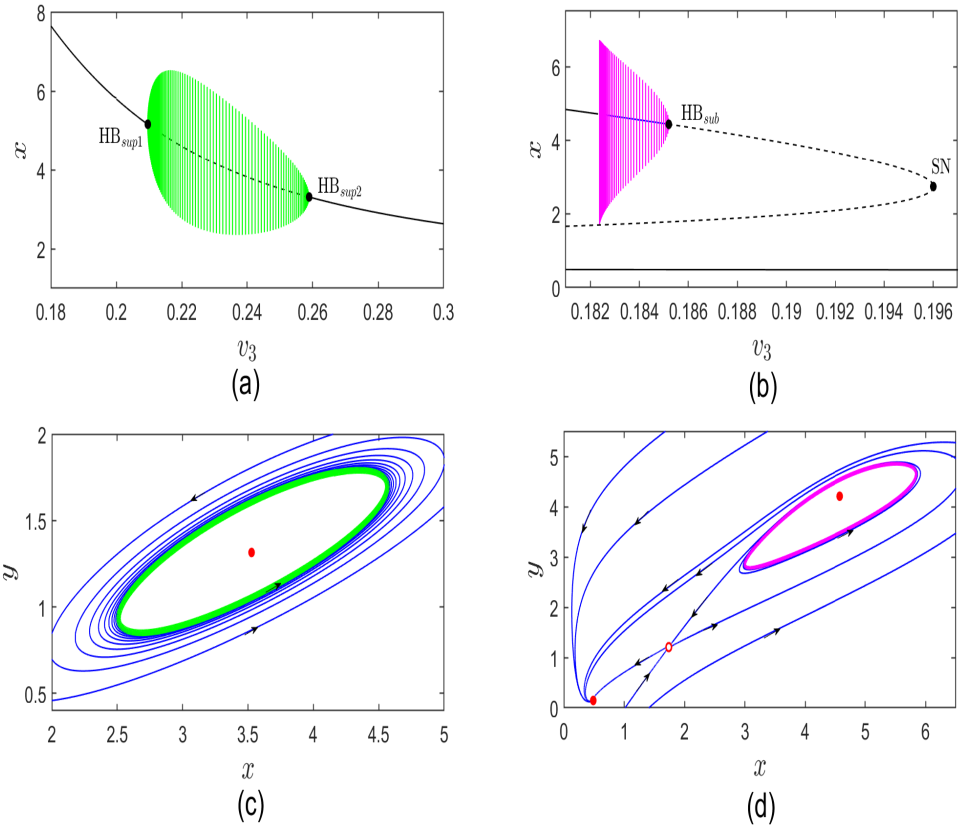

Figure 4. (**a**) – (**b**) Codimension–1 bifurcation diagrams of x with respect to v_3 for $v_1 = 0.8153$, $v_2 = 0.2$, $d_1 = 0.015$, $d_2 = 0.04$, $r_1 = 0.03$, $r_2 = 0.002$, $k_1 = 7$, $k_2 = 3$, $k_3 = 7$ and $v_1 = 0.63$, $v_2 = 0.06$, $v_3 = 0.1838$, $d_1 = 0.034$, $d_2 = 0.025$, $r_1 = 0.011$, $r_2 = 0.001$, $k_1 = 4.5$, $k_2 = 2$, $k_3 = 4$, respectively. Black solid and dashed lines represent stable and unstable equilibria, respectively. HB_{sup1}, HB_{sup1} and HB_{sub} are supercritical and subcritical Hopf bifurcation points. SN denotes the saddle–node bifurcation point. Green and purple vertical lines represent the stable and unstable limit cycles, respectively. (**c**) – (**d**) Phase portraits of x and y. A stable limit cycle (the green line) created by HB_{sup1} at $v_3 = 0.25$ in (a). An unstable limit cycle (the purple line) created by HB_{sub} at $v_3 = 0.1838$ in (b).

4.3. Bogdanov – Takens bifurcation

Apart from codimension–1 saddle–node and Hopf bifurcation, the system (2.1) may undergo codimension–2 Bogdanov–Takens bifurcation at the positive equilibria $E(x_*, y_*)$, which will be analyzed by considering v_3 and d_2 as bifurcation parameters in the next section.

Let v_3^{BT} and d_2^{BT} be two critical values of v_3 and d_2, at which $\det(J(E))\Big|_{(v_3,d_2)=(v_3^{BT},d_2^{BT})} = 0$ and $\mathrm{tr}(J(E))\Big|_{(v_3,d_2)=(v_3^{BT},d_2^{BT})} = 0$. Perturbing v_3 and d_2 by $v_3 = v_3^{BT} + \mu_1$ and $d_2 = d_2^{BT} + \mu_2$ with μ_1 and μ_2 in a small neighborhood of $(0, 0)$, the system (2.1) becomes

$$
\begin{cases}
\dfrac{\mathrm{d}x}{\mathrm{d}t} = r_1 + u_2\dfrac{x^2}{k_1^2+x^2} - v_2 y\dfrac{x}{k_2+x} - d_1 x, \\
\dfrac{\mathrm{d}y}{\mathrm{d}t} = r_2 + (v_3^{BT}+\mu_1)\dfrac{x^2}{k_3^2+x^2} - (d_2^{BT}+\mu_2)y.
\end{cases} \tag{4.1}
$$

Transforming the equilibrium $E(x_*, y_*)$ to the origin $(0, 0)$ by $z_1 = x - x_*$ and $z_2 = y - y_*$, the system (4.1) becomes

$$
\begin{cases}
\dot{z}_1 = a_{10}(\mu)z_1 + a_{01}(\mu)z_2 + a_{20}(\mu)z_1^2 + a_{11}(\mu)z_1z_2 + R_1(z,\mu), \\
\dot{z}_2 = b_{00}(\mu) + b_{10}(\mu)z_1 + b_{01}(\mu)z_2 + b_{20}(\mu)z_1^2 + R_2(z,\mu),
\end{cases} \tag{4.2}
$$

where

$$
\begin{aligned}
&a_{10}(\mu) = \frac{2k_1^2 v_1 x_*}{(k_1^2+x_*^2)^2} - \frac{k_2 v_2 y_*}{(k_2+x_*)^2} - d_1,\ a_{01}(\mu) = -\frac{v_2 x_*}{k_2+x_*},\ a_{20}(\mu) = \frac{k_1^2 v_1(k_1^2-3x_*^2)}{(k_1^2+x_*^2)^3} + \frac{k_2 v_2 y_*}{(k_2+x_*)^3}, \\
&a_{11}(\mu) = -\frac{k_2 v_2}{(k_2+x_*)^2},\ b_{00}(\mu) = r_2 + (v_3+\mu_1)\frac{x_*^2}{k_3^2+x_*^2} - (d_2+\mu_2)y_*,\ b_{10}(\mu) = \frac{2k_3^2(v_3^{BT}+\mu_1)x_*}{(k_3^2+x_*^2)^2}, \\
&b_{01}(\mu) = -(d_2^{BT}+\mu_2),\ b_{20}(\mu) = \frac{k_3^2(v_3^{BT}+\mu_1)(k_3^2-3x_*^2)}{(k_3^2+x_*^2)^3},
\end{aligned}
$$

and $z = (z_1, z_2)^T$, $\mu = (\mu_1, \mu_2)^T$. $R_i(z, \mu) = O(\|z\|^3)$ $(i = 1, 2)$ denotes the power series as to z_1, z_2 with the order 3 and more. The coefficients of $R_i(z, \mu)(i = 1, 2)$ and a_{ij}, b_{ij} smoothly depend on μ_1 and μ_2. According to $b_{00}(0) = 0$, we rewrite the system (4.2) at $\mu_1 = 0$ and $\mu_2 = 0$ in the following form

$$
\frac{\mathrm{d}z}{\mathrm{d}t} = J_0 z + F(z),
$$

where

$$
\textbf{(BT.1)} \qquad J_0 = \begin{pmatrix} a_{10}(0) & a_{01}(0) \\ b_{10}(0) & b_{01}(0) \end{pmatrix} \neq \mathbf{0}\,,
$$

$$
F(z) = \begin{pmatrix} a_{20}(\mu)z_1^2 + a_{11}(\mu)z_1z_2 + R_1(z,\mu) \\ b_{20}(\mu)z_1^2 + R_2(z,\mu) \end{pmatrix}.
$$

Let $a_{10}(0) = a_{10}$, $a_{01}(0) = a_{01}$, $b_{10}(0) = b_{10}$ and $b_{01}(0) = b_{01}$. Since J_0 has two zero eigenvalues, we get $a_{10} + b_{01} = 0$ and $a_{10}b_{01} = a_{01}b_{10}$. Then, we choose $\alpha_0 = \left(1, -\frac{a_{10}}{a_{01}}\right)^T$, $\alpha_1 = \left(0, \frac{1}{a_{01}}\right)^T$ and $\beta_0 = (1, 0)^T$, $\beta_1 = (a_{10}, a_{01})^T$ as the eigenvector and generalized eigenvector with zero eigenvalues for J_0 and J_0^T, respectively, which satisfy $\langle\alpha_0, \beta_0\rangle = \langle\alpha_1, \beta_1\rangle = 1$ and $\langle\alpha_1, \beta_0\rangle = \langle\alpha_0, \beta_1\rangle = 0$. The linearly independent vectors α_0 and α_1 form a basis of $\mathbb{R}^2$. Thus, we make the following transformation

$$
z = \gamma_1\alpha_0 + \gamma_2\alpha_1,
$$

i.e., $\gamma_1 = z_1$, $\gamma_2 = a_{10}z_1 + a_{01}z_2$. Then the system (4.2) becomes

$$
\begin{cases}
\dot{\gamma}_1 = \gamma_2 + c_{20}(\mu){\gamma_1}^2 + c_{11}(\mu)\gamma_1\gamma_2 + R_3(\gamma,\mu), \\
\dot{\gamma}_2 = d_{00}(\mu) + d_{10}(\mu)\gamma_1 + d_{01}(\mu)\gamma_2 + d_{20}(\mu){\gamma_1}^2 + d_{11}(\mu)\gamma_1\gamma_2 + R_4(\gamma,\mu),
\end{cases} \tag{4.3}
$$

where

$$c_{20}(\mu) = a_{20}(\mu) - \frac{a_{10}a_{11}(\mu)}{a_{01}},\ c_{11}(\mu) = \frac{a_{11}(\mu)}{a_{01}},\ d_{00}(\mu) = a_{01}b_{00}(\mu),$$
$$d_{10}(\mu) = a_{01}b_{10}(\mu) - a_{10}b_{01}(\mu), d_{01}(\mu) = a_{10} + b_{01}(\mu),$$
$$d_{20}(\mu) = a_{10}a_{20}(\mu) - \frac{a_{10}^2 a_{11}(\mu)}{a_{01}} + a_{01}b_{20}(\mu),\ d_{11}(\mu) = \frac{a_{10}a_{11}(\mu)}{a_{01}},$$

and $R_{3,4}(\gamma,\mu) = O(\|\gamma\|^3)$ $(\gamma = (\gamma_1,\gamma_2)^T)$. Due to $a_{10} + b_{01} = 0$ and $a_{10}b_{01} = a_{01}b_{10}$, we obtain $d_{00}(0) = d_{10}(0) = d_{01}(0) = 0$.

Next, making the transformations $\eta_1 = \gamma_1$ and $\eta_2 = \gamma_2 + c_{20}(\mu)\gamma_1{}^2 + c_{11}(\mu)\gamma_1\gamma_2 + R_3(\gamma,\mu)$, system (4.3) becomes

$$\begin{cases} \dot{\eta}_1 = \eta_2, \\ \dot{\eta}_2 = e_{00}(\mu) + e_{10}(\mu)\eta_1 + e_{01}(\mu)\eta_2 + e_{20}(\mu)\eta_1{}^2 + e_{11}(\mu)\eta_1\eta_2 + e_{02}(\mu)\eta_2{}^2 + R_5(\eta,\mu), \end{cases} \tag{4.4}$$

where

$$e_{00}(\mu) = d_{00}(\mu),\ e_{10}(\mu) = d_{10}(\mu) + c_{11}(\mu)d_{00}(\mu),\ e_{01}(\mu) = d_{01}(\mu),\ e_{02}(\mu) = c_{11}(\mu),$$
$$e_{20}(\mu) = d_{20}(\mu) + c_{11}(\mu)d_{10}(\mu) - c_{20}(\mu)d_{01}(\mu),\ e_{11}(\mu) = d_{11}(\mu) + 2c_{20}(\mu),$$

and $R_5(\eta,\mu) = O(\|\eta\|^3)$, $\eta = (\eta_1,\eta_2)^T$. Moreover, we have

$$e_{00}(0) = e_{10}(0) = e_{01}(0) = 0,\ e_{20}(0) = d_{20}(0),\ e_{11}(0) = d_{11}(0) + 2c_{20}(0),\ e_{02}(0) = c_{11}(0).$$

And we assume that

$$(\mathbf{BT.2}) \quad e_{11}(0) = d_{11}(0) + 2c_{20}(0) \neq 0,$$

Then making a coordinate shift $\eta_1 = \omega_1 + \xi(\mu)$, $\eta_2 = \omega_2$, where $\xi(\mu) \approx -\frac{e_{01}(\mu)}{e_{11}(0)}$, the system (4.4) reduces to

$$\begin{cases} \dot{\omega}_1 = \omega_2, \\ \omega_2 = f_{00}(\mu) + f_{10}(\mu)\omega_1 + f_{20}(\mu)\omega_1^2 + f_{11}(\mu)\omega_1\omega_2 + f_{02}(\mu)\omega_2^2 + R_6(\omega,\mu), \end{cases} \tag{4.5}$$

where

$$\begin{aligned} &f_{00}(\mu) = e_{00}(\mu) + e_{10}(\mu)\xi(\mu) + \cdots,\ f_{10}(\mu) = e_{10}(\mu) + 2e_{20}(\mu)\xi(\mu) + \cdots,\ f_{02}(\mu) = e_{02} + \xi(\mu) + \cdots, \\ &f_{11}(\mu) = e_{11}(\mu) + 2\xi(\mu) + \cdots, f_{20}(\mu) = e_{20}(\mu) + 3\xi(\mu) + \cdots, \end{aligned} \tag{4.6}$$

and $R_6(\omega,\mu) = O(\|\omega\|^3)$ $(\omega = (\omega_1,\omega_2)^T)$.

Next, introducing a new time variable τ_1 by $\mathrm{d}t = (1 + \theta(\mu)\omega_1)\,\mathrm{d}\tau_1$, $\theta(\mu) = -f_{02}(\mu)$, system (4.5) becomes

$$\begin{cases} \dot{\omega}_1 = \omega_2, \\ \dot{\omega}_2 = h_{00}(\mu) + h_{10}(\mu)\omega_1 + h_{20}(\mu)\omega_1^2 + h_{11}(\mu)\omega_1\omega_2 + R_7(\omega,\mu), \end{cases} \tag{4.7}$$

in which

$$h_{00}(\mu) = f_{00}(\mu),\ h_{10}(\mu) = f_{10}(\mu) - 2f_{00}(\mu)f_{02}(\mu),$$
$$h_{20}(\mu) = f_{20}(\mu) - 2f_{10}(\mu)f_{02}(\mu) + f_{00}(\mu)f_{02}(\mu)^2,\ h_{11}(\mu) = f_{11}(\mu),$$

and $R_7(\omega,\mu) = O(\|\omega\|^3)$.

If the following condition holds,

$$(\mathbf{BT.3}) \quad h_{20}(0) = d_{20}(0) \neq 0,$$

then we introduce the new variables $\tau_2 = \left|\frac{h_{20}(\mu)}{h_{11}(\mu)}\right|\tau_1$, $y_1 = \frac{h_{11}^2(\mu)}{h_{20}(\mu)}\omega_1$, $y_2 = \text{sign}\left(\frac{h_{20}(\mu)}{h_{11}(\mu)}\right)\frac{h_{11}^3(\mu)}{h_{20}^2(\mu)}\omega_2$, the system (4.7) is changed to

$$\begin{cases} \dot{y_1} = y_2, \\ \dot{y_2} = m_{00}(\mu) + m_{10}(\mu)y_1 + y_1^2 + sy_1y_2 + R_8(y,\mu), \end{cases} \tag{4.8}$$

where

$$m_{00}(\mu) = \frac{h_{11}^4(\mu)}{h_{20}^3(\mu)}h_{00}(\mu),\ m_{10}(\mu) = \frac{h_{11}^2(\mu)}{h_{20}^2(\mu)}h_{10}(\mu), \tag{4.9}$$

$$s = \text{sign}\left(\frac{h_{20}(\mu)}{h_{11}(\mu)}\right) = \text{sign}\left(\frac{h_{20}(0)}{h_{11}(0)}\right) = \text{sign}\left(\frac{e_{20}(0)}{e_{11}(0)}\right) = \pm 1,$$

and $R_8(y,\mu) = O(\|y\|^3)$, $y = (y_1, y_2)^T$.

If the following transversality condition holds,

$$(\mathbf{BT.4}) \quad \det\left(\frac{\partial\,(m_{00}, m_{10})}{\partial\,(\mu_1,\mu_2)}\right)_{\mu_1=\mu_2=0} \neq 0,$$

the system (4.1) experiences Bogdanov–Takens bifurcation when $\mu = (\mu_1,\mu_2)$ is in a small neighborhood of $(0,0)$ based on the results in [22]. According to the above discussion, the following theorem is obtained.

Theorem 4.3. *The system* (2.1) *experiences codimension–2 Bogdanov–Takens bifurcation at the positive equilibrium $E(x_*, y_*)$ as (v_3, d_2) varies near $\left(v_3^{BT}, d_2^{BT}\right)$ and the conditions* (**BT.1**)*–*(**BT.4**) *are satisfied. The local representations of the bifurcation curves are given as follows:*
(i) the saddle–node bifurcation curve $SN = \left\{(\mu_1,\mu_2) \mid 4m_{00} - m_{10}^2 = 0\right\}$;
(ii) the Hopf bifurcation curve $H = \{(\mu_1,\mu_2) \mid m_{00} = 0,\ m_{10} < 0\}$;
(iii) the homoclinic bifurcation curve $HL = \left\{(\mu_1,\mu_2) \mid m_{00} = -\frac{6}{25}m_{10}^2 + O\left(m_{10}^2\right),\ m_{10} < 0\right\}$.

Theorem 4.3 is verified by codimension–2 bifurcation diagram of v_3 and d_2 in Figure 5 and phase portraits of x and y in Figure 6 with $r_1 = 0.011$, $r_2 = 0.001$, $v_1 = 0.63$, $v_2 = 0.06$, $k_1 = 4.5$, $k_2 = 2$, $k_3 = 4$ and $d_1 = 0.034$. Through numerical simulation, we find that system (2.1) undergoes Bogdanov–Takens bifurcation at $(v_3, d_2) = (0.3419136, 0.04331208)$, where the conditions (**BT.1**)–(**BT.4**) in Theorem 4.3 are as follows,

$$J_0 = \begin{pmatrix} 0.043312 & -0.034413 \\ 0.054513 & -0.043312 \end{pmatrix} \neq \mathbf{0}$$

$$\left|\frac{\partial\,(m_{00}, m_{10})}{\partial\,(\mu_1,\mu_2)}\right|_{\mu_1=\mu_2=0} = \begin{vmatrix} 0.009438 & 0.563671 \\ -0.163326 & 5.187334 \end{vmatrix} = 0.141019 \neq 0,$$

$e_{11}(0) = -0.002882 \neq 0$, $h_{20}(0) = d_{20}(0) = -0.000125 \neq 0$, and $s = sign(0.042991) = +1$. Moreover, the local representations of the bifurcation curves are given as follows,
(i) the saddle–node bifurcation curve SN

$$\Big\{(\mu_1, \mu_2) \mid 0.0000002763620326\mu_1 - 0.000002097660245\mu_2 \\ + 0.000003702622789\mu_1^2 + 2.500675014\mu_1\mu_2 - 20.19183593\mu_2^2 = 0\Big\};$$

(ii) the Hopf bifurcation curve H

$$\Big\{(\mu_1, \mu_2) \mid 0.000003273285777\mu_1 - 0.00002645487898\mu_2 \\ + 3.14829075\mu_1\mu_2 - 25.22103078\mu_2^2 = 0,\ m_{10} < 0\Big\};$$

(iii) the homoclinic bifurcation curve HL

$$\Big\{(\mu_1, \mu_2) \mid 0.000000690907144\mu_1 - 0.000006244213952\mu_2 \\ - 0.000005734914096\mu_1^2 + 6.251472238\mu_1\mu_2 - 50.47629929\mu_2^2 = 0,\ m_{10} < 0\Big\}.$$

Figure 5 illustrates the curves SN, H and HL in the (μ_1, μ_2) parameter plane. These curves divide the small neighborhood of the origin (0, 0) in the (μ_1, μ_2) plane into four parts, in which the phase portraits of x and y are given in Figure 6 with the trajectory in blue solid lines and the stable and unstable equilibria in red solid and hollow dots, respectively. In order to see the variation around Bogdanov–Takens bifurcation point, phase portraits of x and y are given in insets in Figure 6(a)–(f).
(a) The system (2.1) has a cusp of codimension–2 Bogdanov–Takens bifurcation point E_2^{BT} with another stable node for $(\mu_1, \mu_2) = (0, 0)$ (see Figure 6(a)).
(b) The system (2.1) has a unique stable node when (μ_1, μ_2) lies in region I (see Figure 6(b)).
(c) A saddle and an unstable focus coexist with another stable node when (μ_1, μ_2) enters into region II from region I through the branch SN^- of the curve SN (see Figure 6(c)).
(d) The unstable focus becomes stable and is surrounded by an unstable limit cycle when (μ_1, μ_2) crosses the subcritical Hopf bifurcation curve H into region III (see Figure 6(d)).
(e) A homoclinic loop occurs for (μ_1, μ_2) on the curve HL (see Figure 6(e)).
(f) The unstable limit cycle disappears and three stable equilibria are left when (μ_1, μ_2) crosses the HL curve into region IV (see Figure 6(f)).

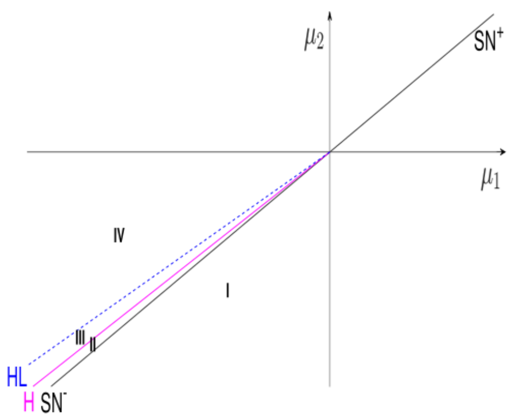

Figure 5. Codimension–2 bifurcation diagram of x with respect to perturbation coefficients μ_1 and μ_2. The origin is codimension–2 Bogdanov–Takens bifurcation point.

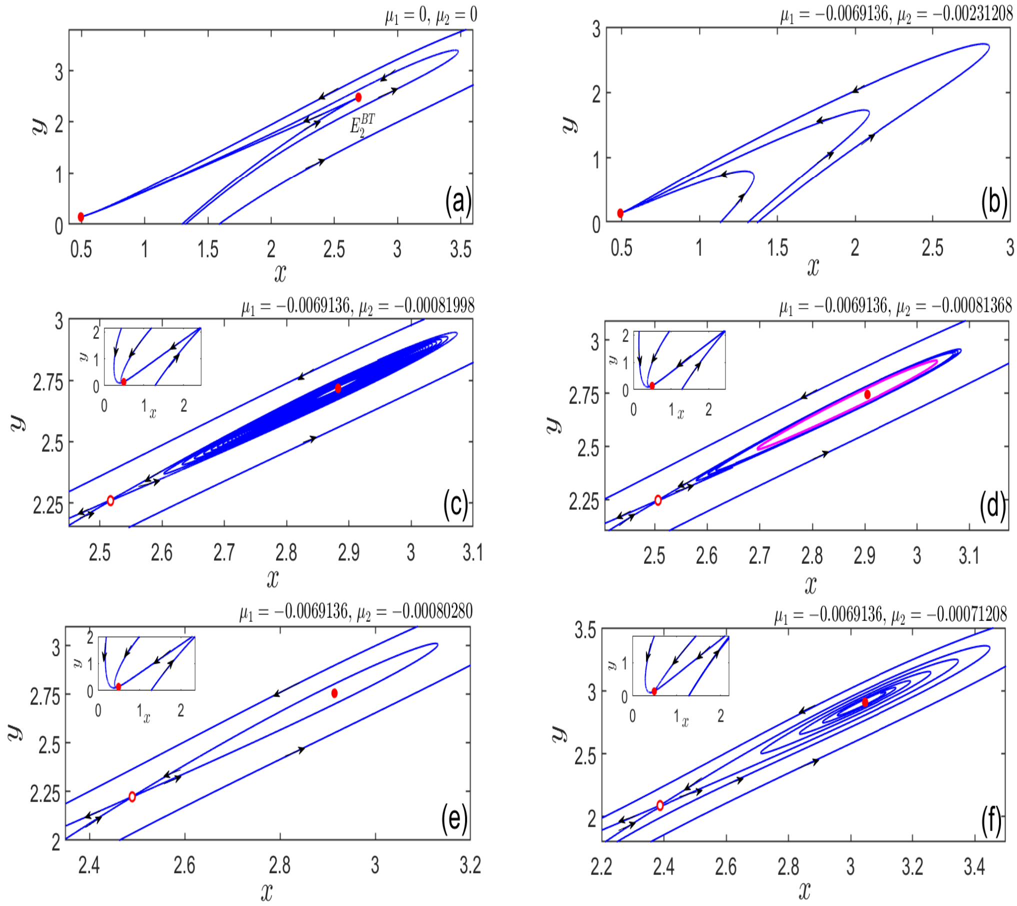

Figure 6. The phase portraits of x and y for typical (μ_1, μ_2) in Figure 5. (**a**) $(\mu_1, \mu_2) = (0, 0)$. (**b**) $(\mu_1, \mu_2) = (-0.0069136, -0.00231208)$ in region I (**c**) $(\mu_1, \mu_2) = (-0.0069136, -0.00081998)$ in region II. (**d**) $(\mu_1, \mu_2) = (-0.0069136, -0.00081368)$ in region III. (**e**) $(\mu_1, \mu_2) = (-0.0069136, -0.00080280)$ on the curve HL. (**f**) $(\mu_1, \mu_2) = (-0.0069136, -0.00071208)$ in region IV.

5. Hopf bifurcation with time delay

In this section, we will investigate the effect of time delay on the stability of the positive equilibrium $E(x_*, y_*)$ in system (2.1).

The system (2.1) is linearized at $E(x_*, y_*)$ as follows,

$$\begin{pmatrix} \dot{x}(t) \\ \dot{y}(t) \end{pmatrix} = \begin{pmatrix} p_{11} & 0 \\ 0 & p_{22} \end{pmatrix} \begin{pmatrix} x(t) \\ y(t) \end{pmatrix} + \begin{pmatrix} 0 & p_{12} \\ 0 & 0 \end{pmatrix} \begin{pmatrix} x(t-\tau_1) \\ y(t-\tau_1) \end{pmatrix} + \begin{pmatrix} 0 & 0 \\ p_{21} & 0 \end{pmatrix} \begin{pmatrix} x(t-\tau_2) \\ y(t-\tau_2) \end{pmatrix} \tag{5.1}$$

where

$$\begin{aligned} p_{11} &= \frac{2k_1^2 v_1 x_*}{(k_1^2 + x_*^2)^2} - d_1, \ \ p_{12} = -\frac{v_2 x_*}{k_2 + x_*}, \\ p_{21} &= \frac{2k_3^2 v_3 x^*}{(k_3^2 + x_*^2)^2}, \ \ p_{22} = -d_2. \end{aligned} \tag{5.2}$$

The characteristic equation of the linearized system (5.1) is

$$\lambda^2 - (p_{11} + p_{22})\lambda + p_{11}p_{22} - p_{12}p_{21}e^{-\lambda(\tau_1+\tau_2)} = 0. \tag{5.3}$$

Assuming that $\lambda = i\omega(\omega > 0)$ is the root of Eq (5.3) and $\tau = \tau_1 + \tau_2$, we get the following equation

$$\omega^2 + (p_{11} + p_{22})i\omega - p_{11}p_{22} + p_{12}p_{21}(\cos\omega\tau - i\sin\omega\tau) = 0. \tag{5.4}$$

Separating the real and imaginary parts of Eq (5.4) results in

$$\begin{cases} p_{12}p_{21}\cos(\omega\tau) + \omega^2 - p_{11}p_{22} = 0, \\ p_{12}p_{21}\sin(\omega\tau) - (p_{11} + p_{22})\omega = 0. \end{cases} \tag{5.5}$$

Thus, $\cos(\omega\tau)$ and $\sin(\omega\tau)$ are given by

$$\begin{cases} \cos(\omega\tau) = \dfrac{p_{11}p_{22} - \omega^2}{p_{12}p_{21}}, \\ \sin(\omega\tau) = \dfrac{(p_{11} + p_{22})}{p_{12}p_{21}}\omega, \end{cases} \tag{5.6}$$

which implies that

$$\omega^4 + (p_{11}^2 + p_{22}^2)\omega^2 + (p_{22}p_{11})^2 - (p_{12}p_{21})^2 = 0. \tag{5.7}$$

The discriminant of Eq (5.7) is

$$\begin{aligned} \Delta_\omega &= \left(p_{11}^2 + p_{22}^2\right)^2 - 4\left((p_{22}p_{11})^2 - (p_{12}p_{21})^2\right) \\ &= \left(p_{11}^2 - p_{22}^2\right)^2 + 4(p_{12}p_{21})^2 > 0. \end{aligned} \tag{5.8}$$

Therefore, Eq (5.7) has two different roots ω_1^2 and ω_2^2, and $\omega_1^2 + \omega_2^2 = -(p_{11}^2 + p_{22}^2) < 0$, $\omega_1^2\omega_2^2 = (p_{22}p_{11})^2 - (p_{12}p_{21})^2$. Therefore, if $(p_{22}p_{11})^2 - (p_{12}p_{21})^2 < 0$, Eq (5.7) has a purely imaginary root $i\omega_0$ and

$$\omega_0 = \sqrt{\frac{-(p_{11}^2 + p_{22}^2) + \sqrt{\Delta_\omega}}{2}}. \tag{5.9}$$

Then, according to Eq (5.6), the critical value of τ is given as follows,

$$\tau_0^{(j)} = \frac{1}{\omega_0}\arccos\left(\frac{p_{11}p_{22} - \omega_0^2}{p_{12}p_{21}}\right) + \frac{2j\pi}{\omega_0},\ j = 0, 1, 2, \cdots. \tag{5.10}$$

Let

$$\tau_0 = min\{\tau_0^{(j)} \big| \ j = 0, 1, 2, \cdots\}. \tag{5.11}$$

Next, we will verify the transversality condition $sign\left\{\left[\dfrac{d\mathrm{Re}(\lambda(\tau))}{d\tau}\right]\Bigg|_{\tau=\tau_0}\right\} \neq 0$. By differentiating both sides of Eq (5.3) with respect to τ, we get

$$\left(\frac{d\lambda(\tau)}{d\tau}\right)^{-1} = -\frac{(2\lambda - (p_{11} + p_{22}))e^{\lambda\tau}}{p_{12}p_{21}\lambda} - \frac{\tau}{\lambda}.$$

At $\tau = \tau_0$, we have

$$\begin{aligned}
&\mathrm{Re}\left(\frac{d\lambda}{d\tau}\right)^{-1} = \mathrm{Re}\left\{-\frac{(2\lambda - (p_{11} + p_{22}))e^{\lambda\tau}}{p_{12}p_{21}\lambda} - \frac{\tau}{\lambda}\right\} \\
&= \mathrm{Re}\left\{\frac{(p_{11} + p_{22})\cos\omega_0\tau_0 + 2\omega_0 \sin\omega_0\tau_0 + i((p_{11} + p_{22})\sin\omega_0\tau_0 - 2\omega_0\cos\omega_0\tau_0)}{p_{12}p_{21}i\omega_0}\right\} \\
&= \frac{1}{(p_{12}p_{21})^2}\{2\omega_0{}^2 + [(p_{11} + p_{22})^2 - 2p_{11}p_{22}]\} \\
&= \frac{1}{(p_{12}p_{21})^2}\sqrt{\Delta_\omega} > 0.
\end{aligned}$$

Hence,

$$sign\left\{\left[\frac{d\mathrm{Re}(\lambda)}{d\tau}\right]\Bigg|_{\tau=\tau_0}\right\} = sign\left\{\mathrm{Re}\left(\frac{d\lambda}{d\tau}\right)^{-1}\Bigg|_{\tau=\tau_0}\right\} > 0.$$

Finally, we have the following theorem based on the Hopf bifurcation theorem [37].

Theorem 5.1. *Let τ_0 and $p_{11}, p_{12}, p_{21}, p_{22}$ be defined by Eqs (5.11) and (5.2), If $(p_{22}p_{11})^2 - (p_{12}p_{21})^2 < 0$, the positive equilibrium $E(x_*, y_*)$ of system* (2.1) *is asymptotically stable for $\tau \in (0, \tau_0]$ and the system* (2.1) *undergoes Hopf bifurcations at $\tau = \tau_0$.*

Theorem 5.1 is verified by the bifurcation diagram of x with respect to τ_2 in Figure 7(a) and phase portraits of x and y in Figure 7 (b)–(d) with $v_1 = 0.86, v_2 = 0.6, v_3 = 0.89, d_1 = 0.017, d_2 = 0.49, r_1 = 0.17, r_2 = 0.004, k_1 = 1.07, k_2 = 0.03$ and $k_3 = 0.42$. For these parameters, the system (2.1) has a unique equilibrium $E(x_*, y_*) = (0.2126, 0.3785)$ and $(p_{22}p_{11})^2 - (p_{12}p_{21})^2 = -0.4940 < 0$, then $\omega_0 = 0.7677$, $\tau_0 = 0.4677$ in Theorem 5.1. Based on Theorem 5.1, the positive equilibrium $E(x_*, y_*) = (0.2126, 0.3785)$ is locally asymptotically stable for $\tau \in (0, \tau_0)$ and the system (2.1) undergoes supcritical Hopf bifurcation at $\tau = \tau_0$, which is accord with bifurcation diagram in Figure 7 (a). In Figure 7 (a), black solid and dashed lines respectively denote stable and unstable equilibria while green dots represent the maxima and minima of stable limit cycle, supcritical Hopf bifurcation HB_{sup} occurs at $\tau_2 = 0.2677 = \tau_0 - \tau_1$ with $\tau_1 = 0.2$. Besides, in the phase diagrams of x and y in Figure 7(b)–(d), red solid and hollow dots denote stable and unstable equilibria, respectively, and blue and green lines respectively denote the trajectory and a stable limit cycle, the positive equilibrium $E(x_*, y_*)$ is stable for $\tau_2 = 0.1 < \tau_0 - \tau_1$ in Figure 7(b); and it lose stability at $\tau_2 = 0.2677 = \tau_0 - \tau_1$ in Figure 7(c); then it become unstable one with the appearance of a stable limit cycle at $\tau_2 = 0.35 > \tau_0 - \tau_1$ in Figure 7(d).

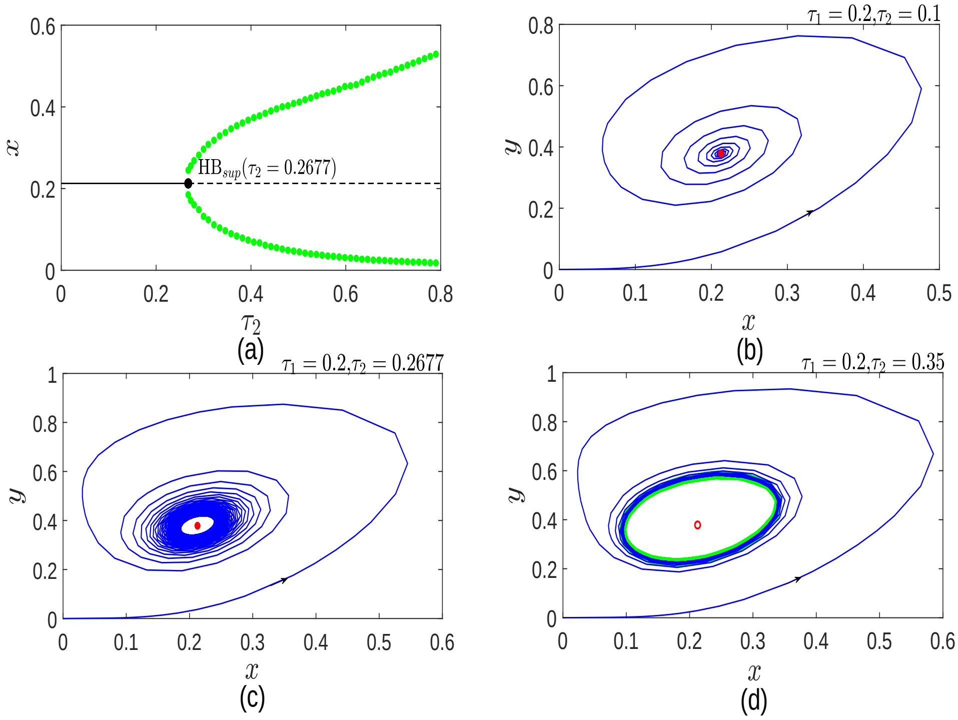

Figure 7. (**a**) Codimension–1 bifurcation diagram of x with respect to τ_2 for $\tau_1 = 0.2$. (**b**)–(**d**) Phase portraits of x and y for $\tau_2 = 0.1 < \tau_0 - \tau_1$, $\tau_2 = \tau_0 - \tau_1 = 0.2677$ and $\tau_2 = 0.35 > \tau_0 - \tau_1$.

6. Conclusions

In this paper, we are mainly concerned with the stability and bifurcation of system (2.1) without and with time delay τ. For $\tau = 0$, the existence of positive equilibria of system (2.1) are analyzed through the Descartes' rule of signs to obtain the conditions under which the system (2.1) has a unique positive equilibrium in Theorem 3.1, which are verified by the nucllines of x and y in system (2.1) in Figure 2. The stability of positive equilibria of system (2.1) without time delay is presented in Table 2 due to the complex expression of the determinant and trace of the Jacobian matrix. For positive equilibria, selecting v_3 as a bifurcation parameter, the conditions of saddle-node and Hopf bifurcation in system (2.1) are given in Theorems 4.1 and 4.2, which gives the first Lyapunov number that determines the stability of limit cycle. These two theorems are verified by codimension-1 bifurcation diagram of x with respect to v_3 in Figures 3 and 4, which include saddle-node bifurcation and supercritical and subcritical Hopf bifurcation, respectively. Furthermore, by choosing two parameters v_3 and d_2 in system (2.1) as bifurcation parameters, we prove that the system exhibits codimension-2 Bogdanov-Takens bifurcation under the conditions in Theorem 4.3, which is obtained by calculating universal unfolding near the cusp. Theorem 4.3 is verified by codimension- 2 bifurcation diagram in Figure 5, which includes Bogdanov-Takens bifurcation point generating the curves of saddle-node, Hopf and homoclinic bifurcation. For $\tau \neq 0$, we find time delay induce the superscribe Hopf bifurcation under the conditions in Theorem 5.1, which is verified by the bifurcation diagram of x with respect to τ_2 and phase portraits of x and y.

Our results give rigorous mathematical proofs of the stability and bifurcation for a two-dimensional p53 GRN to expand the understanding of p53 GRN. Besides, the theoretical analyses of GRNs with noise and space will be further to explored [38–40]. In recent years, fractional-order differential equations (FODEs) are used to describe GRNs because they possess memory, after-affects and hereditary properties, which are more compatible with reality than the integer-order differential equations [41–44]. Therefore, it is worth to explore the stability and bifurcation of GRNs described by three or four dimensional FODEs.

Use of AI tools declaration

The authors declare that they have not used Artificial Intelligence tools in the creation of this article.

Acknowledgments

This work is supported by the National Natural Science Foundation of China (Nos. 12062017 and 12262025), Natural Science Foundation of Inner Mongolia Autonomous Region of China (Grants 2021ZD01), and Program for Innovative Research Team in Universities of Inner Mongolia Autonomous Region of China (No. NMGIRT2008). The authors acknowledge the reviewers for their valuable reviews and kind suggestions.

Conflict of interest

The authors declare that there is no conflict of interest.

References

1. Q. Zhu, J. Shen, F. Han, W. Lu, Bifurcation analysis and probabilistic energy landscapes of two-component genetic network, *IEEE Access*, **8** (2020), 150696–150708. https://doi.org/10.1109/ACCESS.2020.3013615
2. L. Fang, Y. Li, L. Ma, Q. Xu, F. Tan, G. Chen, GRNdb: decoding the gene regulatory networks in diverse human and mouse conditions, *Nucleic Acids Res.*, **49** (2021), D97–D103. https://doi.org/10.1093/nar/gkaa995
3. X. Zhang, X. Zhao, K. He, L. Lu, Y. Cao, J. Liu, et al., Inferring gene regulatory networks from gene expression data by path consistency algorithm based on conditional mutual information, *Bioinformatics*, **28** (2012), 98–104. https://doi.org/10.1093/bioinformatics/btr626
4. T. Yu, X. Zhang, G. Zhang, B. Niu, Hopf bifurcation analysis for genetic regulatory networks with two delays, *Neurocomputing*, **164** (2015), 190–200. https://doi.org/10.1016/j.neucom.2015.02.070
5. B. S. Stikker, R. W. Hendriks, R. Stadhouders, Decoding the genetic and epigenetic basis of asthma, *Allergy*, **78** (2023), 940–956. https://doi.org/10.1111/all.15666
6. B. Huang, M. Lu, M. Galbraith, H. Levine, J. N. Onuchic, D. Jia, Decoding the mechanisms underlying cell-fate decision-making during stem cell differentiation by random circuit perturbation, *J. R. Soc. Interface*, **17** (2020), 20200500. https://doi.org/10.1098/rsif.2020.0500

7. A. Ghaffarizadeh, G. J. Podgorski, N. S. Flann, Applying attractor dynamics to infer gene regulatory interactions involved in cellular differentiation, *Biosystems*, **155** (2017), 29–41. https://doi.org/10.1016/j.biosystems.2016.12.004

8. S. Vyas, A. J. Rodrigues, J. M. Silva, F. Tronche, O. F. Almeida, N. Sousa, et al., Chronic stress and glucocorticoids: from neuronal plasticity to neurodegeneration, *Neural Plast.*, **2016** (2016), 6391686. https://doi.org/10.1155/2016/6391686

9. J. Chrol-Cannon, Y. Jin, Computational modeling of neural plasticity for self-organization of neural networks, *Biosystems*, **125** (2014), 43–54. https://doi.org/10.1016/j.biosystems.2014.04.003

10. Y. Meng , Y. Jin, J. Yin, Modeling activity-dependent plasticity in BCM spiking neural networks with application to human behavior recognition, *IEEE Trans. Neural Networks*, **22** (2011), 1952–1966. https://doi.org/10.1109/TNN.2011.2171044

11. X. Shi, M. Sun, H. Liu, Y. Yao, R. Kong, F. Chen, et al., A critical role for the long non-coding RNA GAS5 in proliferation and apoptosis in non-small-cell lung cancer, *Mol. Carcinog.*, **54** (2015), E1–E12. https://doi.org/10.1002/mc.22120

12. D. Chudasama, V. Bo, M. Hall, V. Anikin, J. Jeyaneethi, J. Gregory, et al., Identification of cancer biomarkers of prognostic value using specific gene regulatory networks (GRN): a novel role of RAD51AP1 for ovarian and lung cancers, *Carcinogenesis*, **39** (2018), 407–417. https://doi.org/10.1093/carcin/bgx122

13. H. C. Lo, J. H. Hsu, L. C. Lai, M. H. Tsai, E. Y. Chuang, MicroRNA-107 enhances radiosensitivity by suppressing granulin in PC-3 prostate cancer cells, *Sci. Rep.*, **10** (2020), 14584. https://doi.org/10.1038/s41598-020-71128-1

14. J. Eliaš, C. K. Macnamara, Mathematical modelling of p53 signalling during DNA damage response: a survey, *Int. J. Mol. Sci.*, **22** (2021), 10590. https://doi.org/10.3390/ijms221910590

15. Q. Zheng, J. Shen, Z. Wang, Pattern formation and oscillations in Reaction-Diffusion model with p53-Mdm2 feedback Loop, *Int. J. Bifurcation Chaos*, **29** (2019), 1930040. https://doi.org/10.1142/S0218127419300404

16. Y. Bi, Q. Liu, L. Wang, W. Yang, X. Wu, Bifurcation and potential landscape of p53 dynamics depending on pdcd5 level and atm degradation rate, *Int. J. Bifurcation Chaos*, **30** (2020), 2050134. https://doi.org/10.1142/S0218127420501345

17. Y. Bi, Z. Yang, C. Zhuge, J. Lei, Bifurcation analysis and potential landscapes of the p53-mdm2 module regulated by the co-activator programmed cell death 5, *Chaos*, **25** (2015), 113103. https://doi.org/10.1063/1.4934967

18. J. Hou, Q. Liu, H. Yang, L. Wang, Y. Bi, Stability and bifurcation analyses of p53 gene regulatory network with time delay, *Electron. Res. Arch.*, **30** (2022), 850–873. https://doi.org/10.3934/era.2022045

19. C. Gao, F. Chen, Dynamics of p53 regulatory network in DNA damage response, *Appl. Math. Modell.*, **88** (2020), 701–714. https://doi.org/10.1016/j.apm.2020.06.057

20. Y. Song, X. Cao, T. Zhang, Bistability and delay-induced stability switches in a cancer network with the regulation of microRNA, *Commun. Nonlinear Sci. Numer. Simul.*, **54** (2018), 302–319. https://doi.org/10.1016/j.cnsns.2017.06.008

21. T. Sun, R. Yuan, W. Xu, F. Zhu, P. Shen, Exploring a minimal two-component p53 model, *Phys. Biol.*, **7** (2010), 036008. https://doi.org/10.1088/1478-3975/7/3/036008

22. L. Perko, *Differential Equations and Dynamical Systems*, 1991. https://doi.org/10.1007/978-1-4684-0392-3

23. B. Hat, M. Kochanczyk, M. N. Bogdal, T. Lipniacki, Feedbacks, bifurcations, and cell fate decision-making in the p53 system, *PLoS Comput. Biol.*, **12** (2016), e1004787. https://doi.org/10.1371/journal.pcbi.1004787

24. Y. A. Kuznetsov, *Elements of Applied Bifurcation Theory*, 1998. https://doi.org/10.1007/b98848

25. D. Mu, C. Xu, Z. Liu, Y. Pang, Further insight into bifurcation and hybrid control tactics of a chlorine dioxide-iodine-malonic acid chemical reaction model incorporating delays, *Match-Commun. Math. Comput. Chem.*, **89** (2023), 529–566. https://doi.org/10.46793/match.89-3.529M

26. Y. Xiang, Y. Jiao, X. Wang, R. Yang, Dynamics of a delayed diffusive predator-prey model with Allee effect and nonlocal competition in prey and hunting cooperation in predator, *Electron. Res. Arch.*, **31** (2023), 2120–2138. https://doi.org/10.3934/era.2023109

27. M. Sui, Y. Du, Bifurcations, stability switches and chaos in a diffusive predator-prey model with fear response delay, *Electron. Res. Arch.*, **31** (2023), 5124–5150. https://doi.org/10.3934/era.2023262

28. C. Wang, F. Yan, H. Liu, Y. Zhang, Theoretical study on the oscillation mechanism of p53-Mdm2 network, *Int. J. Biomath.*, **11** (2018), 1850112. https://doi.org/10.1142/S1793524518501127

29. Y. Bi, Y. Li, J. Hou, Q. Liu, Multiple time delays induced dynamics of p53 gene regulatory network, *Int. J. Bifurcation Chaos*, **31** (2021), 2150234. https://doi.org/10.1142/S0218127421502345

30. J. Xia, X. Li, Bifurcation analysis in a discrete predator-prey model with herd behaviour and group defense, *Electron. Res. Arch.*, **31** (2023), 4484–4506. https://doi.org/10.3934/era.2023229

31. D. Hu, H. Cao, Stability and bifurcation analysis in a predator-prey system with Michaelis-Menten type predator harvesting, *Nonlinear Anal. Real World Appl.*, **33** (2017), 58–82. https://doi.org/10.1016/j.nonrwa.2016.05.010

32. M. Liu, F. Meng, D. Hu, Bogdanov-Takens and Hopf bifurcations analysis of a genetic regulatory network, *Qual. Theory Dyn. Syst.*, **21** (2022), 45. https://doi.org/10.1007/s12346-022-00575-0

33. H. Zhou, B. Tang, H. Zhu, S. Tang, Bifurcation and dynamic analyses of non-monotonic predator-prey system with constant releasing rate of predators, *Qual. Theory Dyn. Syst.*, **21** (2022), 10. https://doi.org/10.1007/s12346-021-00539-w

34. C. Shan, Y. Yi, H. Zhu, Nilpotent singularities and dynamics in an SIR type of compartmental model with hospital resources, *J. Differ. Equations*, **260** (2016), 4339–4365. https://doi.org/10.1016/j.jde.2015.11.009

35. C. Xu, Q. Cui, Z. Liu, Y. Pan, X. Cui, W. Ou, et al., Extended hybrid controller design of bifurcation in a delayed chemostat model, *Match-Commun. Math. Comput. Chem.*, **90** (2023), 609–648. https://doi.org/10.46793/match.90-3.609X

36. J. Sotomayor, Generic bifurcations of dynamical systems, *Dyn. Syst.*, (1973), 561–582. https://doi.org/10.1016/B978-0-12-550350-1.50047-3

37. B. D. Hassard, N. D. Kazarinoff, Y. H. Wan, *Theory and Applications of Hopf Bifurcation*, 1981.
38. P. Wan, Dynamic behavior of stochastic predator-prey system, *Electron. Res. Arch.*, **31** (2023), 2925–2939. https://doi.org/10.3934/era.2023147
39. Y. Hou, C. Wei, Y. Ding, Dynamic analysis of reaction-diffusion dual carbon model considering economic development in China, *Electron. Res. Arch.*, **31** (2023), 2438–2500. https://doi.org/10.3934/era.2023126
40. W. Li, H. Wang, Dynamics of a three-molecule autocatalytic Schnakenberg model with cross-diffusion: turing patterns of spatially homogeneous Hopf bifurcating periodic solutions, *Electron. Res. Arch.*, **31** (2023), 4139–4154. https://doi.org/10.3934/era.2023211
41. C. Xu, Z. Liu, P. Li, J. Yan, L. Yao, Bifurcation mechanism for fractional-order three-triangle multi-delayed neural networks, *Neural Process. Lett.*, **55** (2023), 6125–6151. https://doi.org/10.1007/s11063-022-11130-y
42. C. Xu, D. Mu, Y. Pan, C. Aouiti, L. Yao, Exploring bifurcation in a fractional-order predator-prey system with mixed delays, *J. Appl. Anal. Comput.*, **13** (2023), 1119–1136. https://doi.org/10.11948/20210313
43. P. Li, Y. Lu, C. Xu, J. Ren, Insight into Hopf bifurcation and control methods in fractional order BAM neural networks incorporating symmetric structure and delay, *Cognit. Comput.*, **15** (2023), 1825–1867. https://doi.org/10.1007/s12559-023-10155-2
44. P. Li, X. Peng, C. Xu, L. Han, S. Shi, Novel extended mixed controller design for bifurcation control of fractional-order Myc/E2F/miR-17-92 network model concerning delay, *Math. Methods Appl. Sci.*, **46** (2023), 18878–18898. https://doi.org/10.1002/mma.9597

AIMS Press